Proceedings of the Fifth International Conference on Nanochannels, Microchannels and Minichannels
ICNMM2007
June 18-20, 2007, Puebla, Mexico

ICNMM2007-30216

KEYNOTE PAPER

MODELING AND PREDICTION OF TWO-PHASE REFRIGERANT FLOW REGIMES AND HEAT TRANSFER CHARACTERISTICS IN MICROGAP CHANNELS

Avram Bar-Cohen
TherPES Laboratory
Department of Mechanical Engineering
University of Maryland
College Park, MD 20742

Emil Rahim
TherPES Laboratory
Department of Mechanical Engineering
University of Maryland
College Park, MD 20742

ABSTRACT

This keynote lecture will open with a brief review of the primary two-phase flow regimes and their impact on thermal transport phenomena in tubes and channels. The Taitel and Dukler flow regime mapping methodology will then be described and applied to the two-phase flow of refrigerants and dielectric liquids in microgap channels. The effects of channel diameter, as well as alternative transition criteria, on the prevailing flow regimes in microgaps will be explored along with available criteria for microchannel behavior.Available microgap data will then be shown to reflect the dominance of annular flow and to display a characteristic heat transfer coefficient curve in such configurations. It is found that the heat transfer coefficients in the low-quality annular flow segment of this locus can be predicted by available, microtube correlations, but that the moderate-quality transition to the axially-decreasing segment occurs at substantially

INTRODUCTION

Forced flow of dielectric liquids, undergoing phase change while flowing in a "microgap" channel defined by the spacing between stacked silicon chips and/or circuit boards – as in Figure 1 - is a promising candidate for the thermal management of advanced semiconductor devices. In the absence of proven, first-principles, predictive relations for two-phase heat exchangers, empirically-derived correlations must be used to determine the heat transfer coefficients, pressure drops, and dryout limits prevailing in such miniature passages. However, the paucity and large variance in the currently available two-phase data for fluorocarbon dielectric liquids severely compromise the accuracy of such predictions. Considerable insight, and some greater confidence in the application of traditional thermofluid correlations to microgap flow, can be obtained by examining the prevailing flow regimes and associated heat transfer behavior of microgap channels.

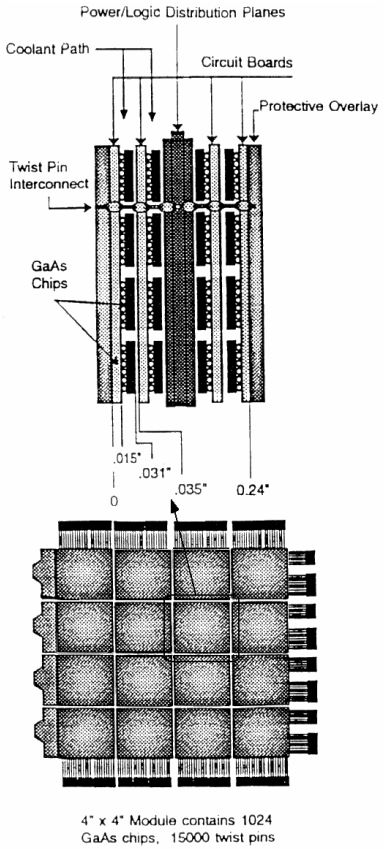

Figure 1: Cray 3 Two-Phase Gas-Assisted Microgap Cooled Module (Bar-Cohen et al 1995)

TWO-PHASE FLOW REGIMES

The flow of vapor and liquid in a channel can take various forms depending on the distribution and extent of "aggregation" of the two phases, with each distinct vapor/liquid distribution referred to as a "flow regime." Four primary two-phase flow regimes: Bubble, Intermittent, Annular, and Stratified, as well as numerous sub-regimes, have been identified in the literature.(Hetsroni 1982). Bubble flow is associated with a uniform distribution of small spherical bubbles within the liquid phase. Intermittent flow is characterized by the flow of liquid "plugs" separated by elongated gas bubbles – often in the shape of "slugs" or bullets – though sometimes more chaotically mixed. In Annular flow, a relatively thin liquid layer flows along the channel walls, while the vapor flows in the center of the channel, creating a vapor "core" which may also contain entrained droplets. In vertical channels with heat addition, where the vapor content increases in the flow direction, as shown in Figure 2, The Bubble regime is followed sequentially by the Intermittent and Annular regimes.

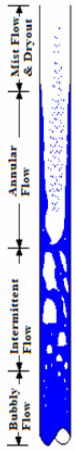

Figure 2: Dominant two-phase flow regimes in a vertical channel**.**

In horizontal or near-horizontal, channels – in addition to the three regimes encountered in vertical channels – two phase flow may also occur in a Stratified pattern in which the liquid flows along the lower surface and the vapor above. This Stratified flow pattern generally occurs at relatively low liquid and vapor flow rates and, as the flow rates increase, transitions into Intermittent or Annular flow.

In a uniformly heated horizontal channel, as seen in Figure 3 , the entering liquid flow may begin in the Stratified regime, progress into the Intermittent, then Bubble regimes, then it may progress into the Intermittent regime again, and experience Annular flow for much of the length of the channel.

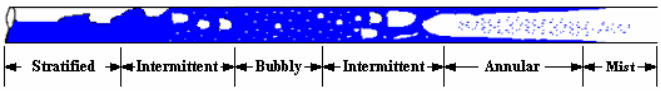

Figure 3: Dominant two-phase flow regimes in a horizontal channel.

HEAT TRANSFER PARAMETERS

The paucity of currently available microchannel two-phase data and the large inherent parametric variations in the essential parameters, most notably in the heat transfer coefficient, as reflected in Figure 4, have motivated efforts to use regime-driven correlations to achieve significant improvements in the predictability of two-phase flow parameters, beyond the current typical range of ± 25% even in well studied geometries. Several recent studies provide direct evidence of the link between flow regimes and key two-phase parameters, including the Critical Heat Flux and the prevailing heat transfer coefficients, and inspire confidence that regime-informed approaches can succeed in improving the predictive accuracy of two-phase formulations.

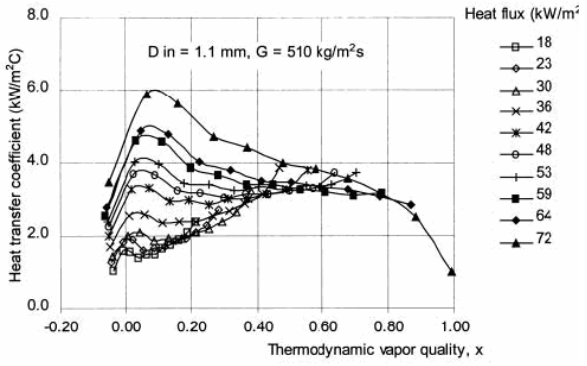

Figure 4: Heat Transfer Coefficient Variations in Typical Two-Phase Mini-tube (Lin et. al. 2001)

The dependence of flow boiling Critical Heat Flux on the prevailing flow regimes was investigated by Bar-Cohen et al, (2005) using a 4150 point, steam-water CHF database compiled by Columbia University and sorted using the Taitel and Dukler mechanistic flow regime mapping methodology (Taitel, 1990). This methodology uses simple hydrodynamic principles to predict the flow regime for a given set of local liquid-vapor conditions and will be discussed in greater detail later in this paper. Table 1 shows the parametric range of this tube and rod bundle data, as well as the prevailing flow regimes based on the Taitel and Dukler model. It may also be seen that, while much of the data is for macrochannels in conventional steam generators, the database does include values for a relatively small, 1mm diameter, 25mm long tubes, operating at near-atmospheric pressure in the Atomic Energy Establishment – Winfrith (AEEW) facility.

Once sorted by regime, the Columbia University CHF data was plotted against vapor thermodynamic quality and inspected for any mechanistic change corresponding to a flow regime transition predicted by the Taitel and Dukler model. It is to be noted that most of the CHF data was identified as being in Annular flow, with very little data ascribed to either Bubble or Intermittent flow. Nevertheless, as may be seen in Figures 5 and 6, the CHF was found to vary linearly with quality, in distinct segments, with a sharp discontinuity and change in slope between data points found to reside in the Bubble regime and those in the Annular flow regime. Figure 5 also reveals a possible inflection point for an intermittent flow

regime transition, but the number of such data points is too small to establish the slope of the CHF locus in this regime. Thus, within each flow regime, CHF appears to display a similar dependence on quality suggesting a consistent "boiling crisis" mechanism, while a change in flow regime appears to alter the functional dependence of CHF on quality and, hence, the underlying mechanism of CHF.

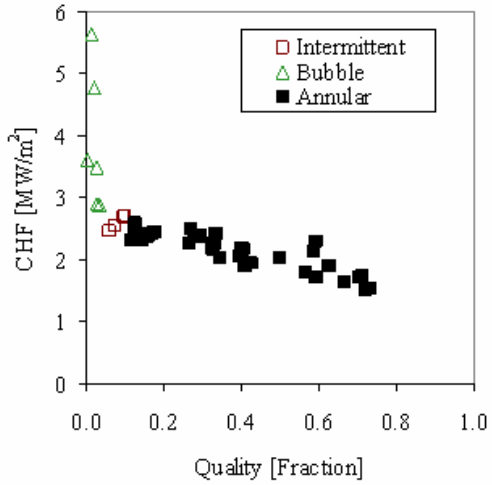

Figure 5: AEEW regime-sorted CHF vs. quality data for varying mass flux – 68 bars, subcooling of 170-300 kJ/kg, pipe diameters of 9-13 mm, and lengths of 1.4-2.0 m. (Bar-Cohen et al, 2005)

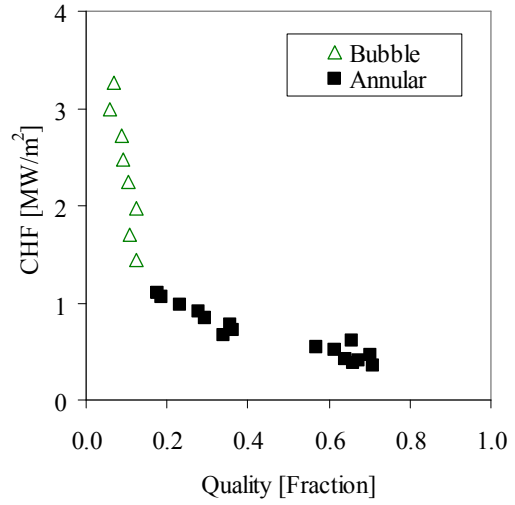

Figure 6: KTH regime-sorted CHF vs. quality data for varying mass flux - pressure of 140 bars, subcooling of 480-573 kJ/kg, pipe diameter of 10 mm, and length of 3 m.(Bar-Cohen, et al 2005)

The Bar-Cohen et al (2005) analysis also included a statistical comparison between the predictions of four generalized correlations: Biasi (1967), Bowring (1972), Katto and Ohno (1984), and Kim and Lee (1997) and the measured CHF data sorted into ten equal segments of vapor quality and sorted by flow regimes.

Table 1: Parametric Range and Flow Regimes of CHF Databases

Database Name	Description	Number of Data Points		
		Total	Regime	
Base	AE177, AEEW, KTH Databases	4109	Annular	3511
			Bubble	381
			Intermittent	217
KLK	Data within the range of the Kim/Lee and Katto/Ohno Correlations	4043	Annular	3462
			Bubble	381
			Intermittent	200
BOW	Data within the range of the Bowring Correlation	3773	Annular	3230
			Bubble	348
			Intermittent	195
BIA	Data within the range of the Biasi Correlation	3495	Annular	3063
			Bubble	254
			Intermittent	178

As may be seen in Figure 7, the largest ε_{RMS} errors – defined as

$$\varepsilon_{RMS} = \sqrt{\sum_{i=1}^{n} \frac{\varepsilon_i^2}{n}}$$

$$\varepsilon_i = \frac{(CHF_{predicted} - CHF_{measured})}{CHF_{measured}}$$

for all the correlations occurred at low qualities (<0.1). For qualities between 0.2 and 0.6, the generalized correlations performed more impressively and consistently with the ε_{RMS} results in this range being the lowest for all but the Katto-Ohno correlation, which did better for some higher quality ranges, while the Biasi correlation did generally poorly in the KLK database. The ε_{RMS} results for the Bowring and Kim-Lee correlations drifted back up at higher qualities (>0.7). In contrast, the predictions of the Biasi and the Katto-Ohno correlations tended to improve at high qualities.

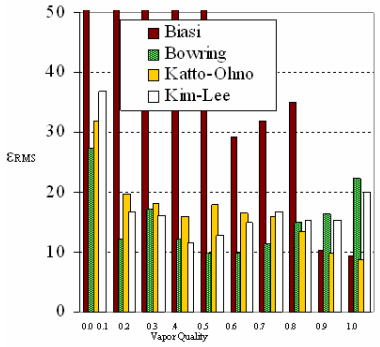

Figure 7: KLK dataset ε_{RMS} results [%] from the quality-sorted CHF comparison (Bar-Cohen et al 2005)

Turning to the flow-regime based comparisons, displayed in Figure 8, the ε_{RMS} in each regime are seen to differ widely

(by as much as a factor of 5) among the correlations and the results for the same correlation vary significantly from regime to regime. Examining the fidelity of the best overall flow boiling CHF correlation in this database, that due to Bowring, it is seen that the discrepancy is lowest in the Bubble regime at approximately 10%, rising to 24% in the Intermittent regime, and decreasing to just 15% in the annular flow regime.

The relatively small discrepancies of the Bowring, as well as Katto-Ohno, correlation of data identified as falling in the Bubble regime, appear to contradict the quality-sorted results, indicating that the largest ε_{RMS} results occurred in the lowest quality band. The authors explained that this apparent contradiction resulted from the low quality data identified as either annular or intermittent flow. It is the annular and intermittent flow data at low qualities in the quality-sorted study that increases the ε_{RMS} value. This result suggests that despite its common use as the sole independent variable in many CHF correlations, vapor quality does not uniquely characterize CHF. correlations.

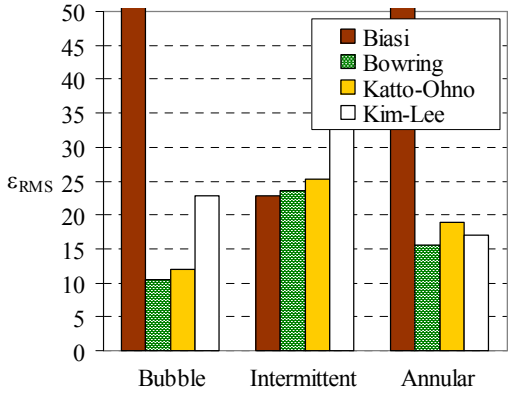

Figure 8: KLK dataset ε_{RMS} results [%] from the regime-sorted CHF comparison.

The importance of flow regime in determining the heat transfer coefficients in two-phase flow was investigated in a recent study by Ghajar et al (2006), who performed a systematic investigation of two-phase heat transfer in a 27.9 mm stainless steel horizontal pipe with a length to diameter ratio of 100. They used air-water flow and aimed at finding a heat transfer correlation that accounts for the flow pattern in the pipe. The two-phase heat transfer coefficient was found to be influenced by the flow pattern – through a flow pattern factor, Fp introduced into the correlation - the superficial liquid Reynolds number, Re_{LS} ,(liquid flow rate), and the superficial gas Reynolds number, Re_{GS}, (gas flow rate). The flow pattern factor was defined as:

$$F_P = \tilde{S}^2_{L,eff} = \left(\frac{S_{L,eff}}{\pi D}\right)^2 = (1-\alpha) + \alpha F_S^2$$

Where F_s is the shape factor defined as:

$$F_S = \frac{2}{\pi}\tan^{-1}\left(\sqrt{\frac{\rho_G (u_G - u_L)^2}{g D(\rho_L - \rho_G)}}\right)$$

regimes. The Homogeneous 1 and 2 correlations offered the best agreement with the Bubble flow data and worst with

Ghajar et al. carefully mapped and photographed the prevailing flow regimes in their 30mm horizontal pipe as presented in Figure 9. While the Stratified and Annular regimes are easily identified, the Intermittent regime is seen to include a large number of sub-regimes and to dominate the two-phase behavior of this pipe in the range tested.

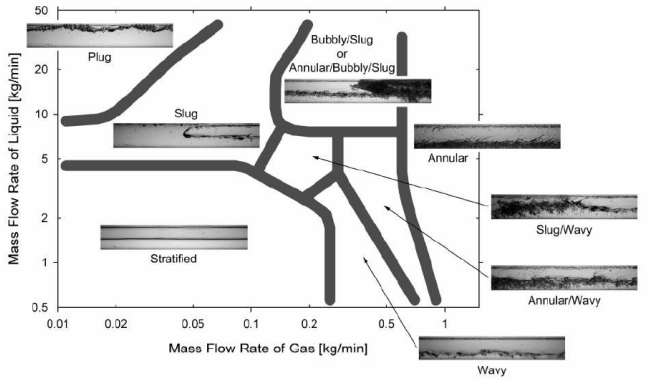

Figure 9: Flow Regime Map for 30mm Horizontal Pipe (Ghajar et al. 2006)

In the data gathered by Ghajar et al., the heat transfer coefficient was found to increase at low Re_{GS}, which corresponds to the Intermittent-slug flow regime, then experiences a change of slope when approaching Annular flow, and continues to shift to higher values as the Re_{GS} increases further and enters into the Annular flow regime. The heat transfer correlation proposed by the authors hence takes the following form

$$h_{TP} = F_P h_L \left\{1 + C\left[\left(\frac{x}{1-x}\right)^m \left(\frac{1-F_P}{F_P}\right)^n \left(\frac{\mathrm{Pr}_G}{\mathrm{Pr}_L}\right)^P \left(\frac{\mu_G}{\mu_L}\right)^q\right]\right\}$$

where h_L comes from the Sieder and Tate (1936) correlation for turbulent flow given as:

$$h_L = 0.027\,\mathrm{Re}_L^{4/5}\,\mathrm{Pr}_L^{1/3}\left(\frac{k_L}{D}\right)\left(\frac{\mu_B}{\mu_W}\right)_L^{0.14}$$

Momoki et al. (2000) explored the potential for using flow regime information to improve the predictive accuracy of five commonly used correlations for the frictional pressure drop component in gas-liquid two-phase flow in a horizontal smooth pipe. The correlations were: Homogeneous model 1, Homogeneous model 2, Chisholm (1973), Martinelli-Nelson (1948), and Thom(1964). Homogeneous models 1 and 2 used the following expressions respectively:

$$\phi^2_{LO} = \{1 + x(\rho_L/\rho_G - 1)\}$$

and

$$\phi^2_{LO} = \{1 + x(\rho_L/\rho_G - 1)\}\{1 + x(\mu_L/\mu_G - 1)\}^{0.25}$$

Momoki et al. compared the mentioned correlations with 460 data points that included both diabatic and adiabatic data of steam-water, air-water, R134a, R22, and R114. The tube diameters ranged from 7.9 mm to 24.3 mm. The datasets were sorted by flow regimes according to Taitel and Dukler (Taitel 1990) prediction methods. It was observed that the agreement of the data with each correlation varied widely across flow

Intermittent data. The Chisholm correlation was found to be worst for Annular and best for Intermittent flow. The Thom

correlation was worst for Intermittent and best for Bubble flow, and the Martinelli-Nelson correlation was found to be the best for Intermittent and worst for Bubble.

FLOW REGIME MAPS

An appreciation for the dependence of thermofluid parameters on the form, as well as extent, of aggregation of each phase led early researchers to describe and map the vapor-liquid flow regimes prevailing in channels used to generate and/or transport two-phase mixtures. Earliest among these was the empirical flow regime map developed by Baker (1954) and numerous other attempts to develop a generalized flow regime map followed; Mandhane et al. (1974), Taitel and Dukler (1976), and Weisman et al. (1979).

Most noteworthy among these was the pioneering effort by Taitel and Dukler, defining and mapping the four predominant flow regimes (Stratified, Intermittent, Bubble, and Annular) with superficial gas and superficial liquid coordinates. After considerable additional contributions by Taitel, Dukler, Barnea, and Shoham, in 1990 this effort culminated in the "unified model" for predicting flow regime transitions in channels of any orientation, based on simple physical criteria and using familiar two-phase non-dimensional groupings (Taitel 1990), as shown in Figures 10 and 11.

Figure 10 presented the transition boundaries of Taitel-Dukler Unified model within the Stratified flow regime and between Stratified and Annular regimes in terms of the non-dimensional liquid height and parameters K, F, or Z or W.

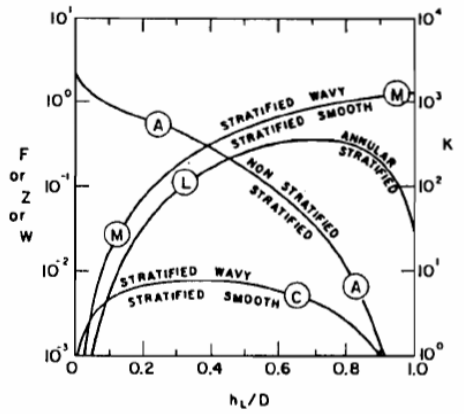

Figure10: Transition boundaries within the Stratified Flow and from between Stratified and Annular according to Taitel and Dukler model. (Taitel, 1990)

Figure 11 presents a generalized map for annular transition in terms of X and Y parameters, being the Martinelli parameter and the inclination parameter, respectively defined as:

$$X = \left[\frac{(dP/dx)_L^S}{(dP/dx)_G^S}\right]^{1/2}$$

$$Y = \frac{(\rho_L - \rho_G)\, g \sin\alpha}{\left|(dP/dx)_G^S\right|}$$

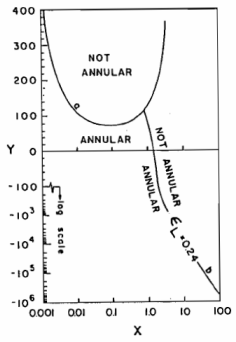

Figure 11: generalized map for Annular transition (Taitel 1990)

.

Table 2: the non-dimensional parameters governing the major transition boundaries in Taitel-Dukler unified model flow regime map.

Curve	Transition	Mechanism	Equation
A	Stratified to non-Stratified	Kelvin-Helmholtz instability	$F = \sqrt{\frac{\rho_G}{(\rho_L-\rho_G)}}\frac{U_{GS}}{\sqrt{D_g\cos\beta}}$ $F^2\left[\frac{1}{C^2}\frac{(u_G/u_{GS})^2 D(dA_L/dh_L)}{A_G}\right]<1$
B	From Bubble	e>0.25	$u_{LS} = u_{GS}\frac{1-\varepsilon}{\varepsilon} - (1-\varepsilon)u_o\sin\beta$
C	Stratified smooth to Stratified Wavy	Jeffreys, wind-wave interaction	$K > \frac{2}{(u_G/u_{GS})\sqrt{u_L/u_{LS}}\sqrt{s}}$ S is an empirical sheltering coefficient, (Benjamin 1968), used here as 0.01
D	From Dispersed Bubble	Turbulent fluctuations and buoyancy	$d_C = (0.725+4.15\varepsilon^{1/2})\left(\frac{\sigma}{\rho_L}\right)^{3/5} k^{-2/5}$ $d_{CD} = 2\left[\frac{0.4\sigma}{(\rho_L-\rho_G)g}\right]^{1/2}$ $d > d_{CB} = \frac{3}{8}\frac{\rho_L}{\rho_L-\rho_G}\frac{f_M\, u_M^2}{g\cos\beta}$
G	From Dispersed Bubble	ε>0.52	$u_{LS} = u_{GS}\frac{1-\varepsilon}{\varepsilon}$
H	Slug – Churn	ε_S>0.52	$\varepsilon_S = 0.058\left[d_C\left(\frac{2f_M}{D}u_M^2\right)^{2/5}\left(\frac{\rho_L}{\sigma}\right)^{3/5} - 0.725\right]^2$
J	From Annular	High void fraction or instability	$\frac{\varepsilon_L}{R_{\max}} = \frac{A_L}{AR_{\max}} > 0.5$ Or Simultaneous solution of the equations 1, 2, and 3
L	Stratified to Annular	Trajectory of torn drops	$u_L^2 > \frac{g\,D\left(1-\frac{h_L}{D}\right)\cos\beta}{f_L}$
M	Stratified smooth to Stratified Wavy	Fr>1.5	$Fr = \frac{u_L}{\sqrt{g\,h_L}} > 1.5$ or $W = \frac{U_{LS}}{\sqrt{gD}} > 1.5\sqrt{\frac{h_L}{D}}\frac{A_L}{A}$
N	Elongated bubble - slug	$\varepsilon_S = 0$	$\varepsilon_S = 0.058\left[d_C\left(\frac{2f_M}{D}u_M^2\right)^{2/5}\left(\frac{\rho_L}{\sigma}\right)^{3/5} - 0.725\right]^2$

$$\tau_i = 0.5 f_i \rho_G \frac{u_{GS}^2}{\left[1-\frac{2\delta}{D}\right]^4} \quad \text{(eq 1)}$$

Eq. 1 represents the shear stress applied from the vapor core on the liquid film in Annular flow.

$$\tau_i = \left[g(\rho_L-\rho_G) D \sin\beta\left(\frac{\delta}{D}-\left[\frac{\delta}{D}\right]^2\right)\right]\left[1-2\frac{\delta}{D}\right]+\frac{1}{32}C_L \rho_L\left[\frac{D}{\nu_L}\right]^{-n} u_{LS}^{(2-n)}\left[\frac{1-\frac{2\delta}{D}}{\left(\frac{\delta}{D}-\left[\frac{\delta}{D}\right]^2\right)^2}\right] \quad \text{(eq. 2)}$$

Eq 2 defines the shear stress required in order to maintain stability in the liquid film and maintain the annular flow.

$$g(\rho_L-\rho_G) D \sin\beta\left[\left(1-2\frac{\delta}{D}\right)^2-2\left(\frac{\delta}{D}-\left[\frac{\delta}{D}\right]^2\right)\right]-\left[\frac{1}{16}C_L \rho_L\left(\frac{D}{\nu_L}\right)^{-n} u_{LS}^{(2-n)}\left(\frac{\frac{\delta}{D}-\left[\frac{\delta}{D}\right]^2+\left[1-2\frac{\delta}{D}\right]^2}{\left[\frac{\delta}{D}-\left(\frac{\delta}{D}\right)^2\right]^3}\right)\right]=0$$

(eq 3)

Thus, for example, a simultaneous solution of Eqs. 1 and 2, that agrees with Eq. 3, provides the transition criteria for moving away from Annular flow and establishes boundary "J"

It is to be noted that the specific formulations used in developing the regime transition criteria reflect the distinction between surface tension driven regimes, such as Bubble and Intermittent flow, and shear force driven regimes, such as Stratified and Annular flow. The models contain little empiricism, and, therefore, can be applied to most fluids and be extrapolated to conditions other than the specific ones that were used in the experimental verification of the approach (Shoham, 1982, Taitel and Dukler, 1987). It would, thus, appear that the Taitel and Dukler mapping methodology could also be applied to microgap channels with evaporating refrigerants and dielectric liquids, of particular interest to this study.

In embracing the use of this flow regime map, it must, nevertheless, be recognized that the Taitel-Dukler methodology relies on adiabatic models that ignore the thermal interactions between phases, the pipe, and the environment which are present in diabatic systems, in which heat is added or extracted from the flowing two-phase mixture. Such an adiabatic model can provide a reasonable prediction of flow regimes if the applied heat flux is low, but high wall heat flux could be expected to shift the transition boundaries for both the Bubble/Intermittent and Stratified/Intermittent interfaces in comparison to that predicted by an adiabatic model (Bar-Cohen et al, 1987). Nevertheless, the model has proven to be exceedingly useful and has demonstrated its first-order accuracy in numerous studies, including those performed by Taitel and Dukler (1987), and Frankum et al (1997).

It is, thus, this physics-based flow regime mapping approach that appears to offer the best basis for determining the prevailing flow regimes in refrigerant flow within microgap channels and for facilitating the extrapolation of available macro-tube water-based correlations to such dielectric liquid microgap coolers.

Figure 12 displays an example of a Taitel and Dukler flow regime map developed in this study for R113 flowing in a horizontal 1mm hydraulic diameter channel, in which the zones occupied by the four primary flow regimes are identified and the locus traversed by the data presented in Yang and Fujita (2004) are shown on the superficial velocity coordinates. In the Stratified flow regime, seen in the lower left corner of the map and encountered only in horizontal or slightly inclined channels at relatively low liquid and vapor superficial velocities, gravity acts to separate the phases, with the liquid flowing along the bottom of the channel and the vapor along the top.

Following Taitel and Dukler, it may be argued that increasing the superficial liquid velocity, as can be caused by a higher liquid flow rate, will lead to a thicker layer of liquid in the channel and allow waves which develop on the liquid–vapor interface to more easily reach the top of the channel and form liquid "bridges" that can then "trap" vapor slugs and produce the phase distribution associated with the Intermittent (slug) flow regime. For the conditions of Fig 13, this transition occurs at a superficial liquid velocity of 0.02 m/s for a superficial gas velocity of 0.1 m/s.

Further increasing the superficial liquid velocity, while keeping the superficial gas velocity constant at 0.1 m/s, will force the liquid to occupy more and more of the channel volume, disrupting the vapor slugs, creating dispersed bubbles, and leading to the appearance of Bubble flow. The Taitel and Dukler model predicts this transition to occur at a superficial liquid velocity of 1 m/s and places the Bubble regime across the top of the flow regime map.

Selecting a point deeper in the Bubble regime, with a superficial liquid velocity of 2 m/s and a superficial gas velocity of 0.1 m/s, and assuming downstream net vapor generation, as will occur in an evaporator, leads to a progressive increase in the superficial gas velocity along with growth in the number and size of the vapor bubbles. These bubbles can then be expected to agglomerate into slugs and lead to a transition into the Intermittent flow regime – predicted by Taitel and Dukler to occur - at a superficial gas velocity of approximately 2.5 m/s.

With a further increase in the flow quality and, therefore, the superficial gas velocity - to an approximate value of 15 m/s - the liquid bridges separating the vapor slugs can no longer be sustained; the vapor breaks through the liquid plugs, pushing this liquid volume into the liquid layer flowing along the channel walls and transitioning into the Annular flow regime. To sustain the annular flow regime, the vapor velocity must then be capable of providing sufficient shear stress to prevent the liquid film from rupturing or - for a horizontal channel - separating by gravity from the upper wall. At high flow qualities the necessary shear force is available and in a diabatic channel experiencing evaporation, the Annular regime persists until all the liquid is evaporated.

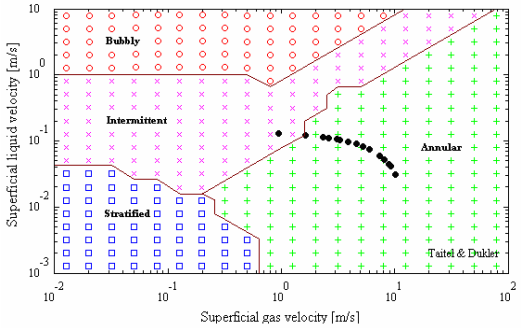

Figure 12: Taitel-Dukler Flow Regime Map for 1mm Refrigerant Microgap Channel [Yang & Fujita (2004), R113, G=200 kg/m^{2}s, q"=50 kW/m^2, D_h= 976 micron single channel.]

As has been previously noted, the physics-based models used in the Taitel and Dukler flow regime maps would appear to provide a firm basis for extrapolation of the flow regime predictions to conditions and fluids other than the water-air and water-steam mixtures flowing in the 2.5cm and larger pipes used in the development of the mapping methodology.

It is, thus, instructive to compare and contrast Taitel and Dukler flow regime maps for both water and R113 flowing in channels with diameters from 100 mm down to 0.1 mm. Fig 14, 15 provide the flow regime maps for the refrigerant R113 in a horizontal and vertical channel, respectively, and display the loci for mass fluxes of 50, 100, 200, and 400 kg/m^{2}s. Most interestingly, in Fig 13, as the channel diameter decreases from 100 mm to 0.1 mm, the Stratified zone is seen to shrink and the Annular (as well as the Bubble) regime grow to include the operating domain for all 4 mass fluxes.

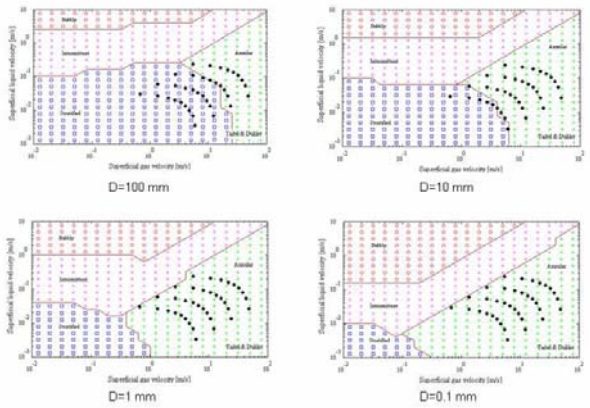

Figure 13: T-D flow regime maps of R113 flowing in a horizontal channel in diameters ranging from 100 mm to 0.1 mm.

A similar outcome is seen for the vertical channel of Figure 14, in which - for the smallest channels - the Annular regime expands into the Intermittent regime and comes to dominate the superficial velocity domain associated with the loci of the four mass fluxes. It may, thus, be anticipated that annular flow will define the thermofluid characteristics of refrigerants flowing in microchannel and microgap coolers, with channel hydraulic diametrs of 1mm or less.

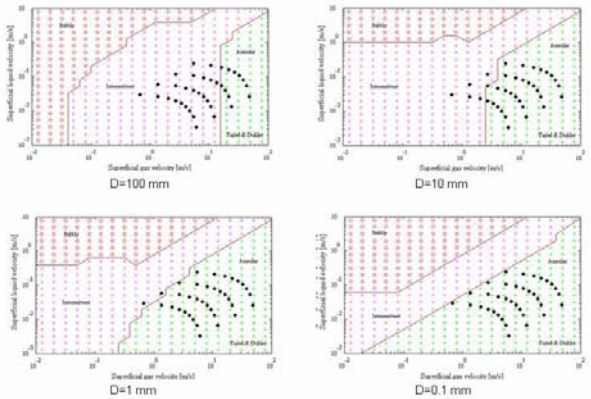

Figure 14: T-D flow regime maps of R113 flowing a in vertical channel in diameters ranging from 100 mm to 0.1 mm

Figures 15 and 16 provide the flow regime maps for water flowing in channels with diameters varying from 100 mm to 0.1 mm. It can be seen that Water flow experiences very similar phenomena as of the refrigerant R113, and a similar conclusion can be drawn for water as for R113. However, it is noted that transitions from Stratified to Annular and Intermittent to Annular occur at a lower vapor quality for water than that for R113.

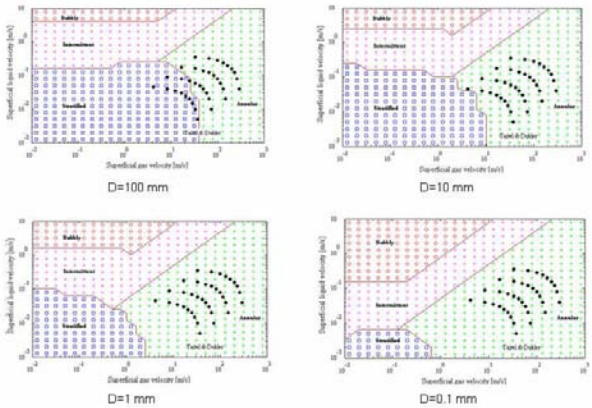

Figure 15: T-D flow regime maps of Water flowing in a horizontal channel in diameters ranging from 100 mm to 0.1 mm

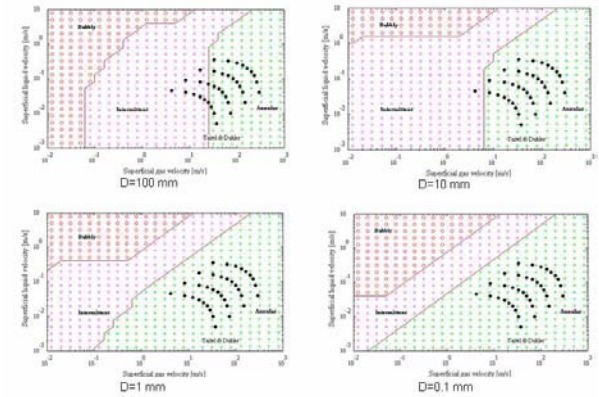

Figure 16: T-D flow regime maps of Water flowing in a vertical channel in diameters ranging from 100 mm to 0.1 mm

WEISMANN INTERMITTENT-ANNULAR TRANSITION CRITERIA

In addition to the Taitel and Dukler mapping methodology, the literature describes other approaches to the identification of two-phase flow regime transitions. Given the importance of the Intermittent-to-Annular transition to the flow of refrigerants in microgap channels, it is appropriate to single out the work of Weismann et al (1979) who correlated this transition in terms of the Froude number and the Kutadelaze number. The boundary between these two regimes in the data gathered by these investigators, as well as data of Simpson et. al (1977), were well fitted by:

$$1.9(V_{SG}/V_{SL})^{1/8} = Ku^{0.2}Fr^{0.18} = \left(\frac{V_{SG}\rho_G^{1/2}}{[g(\rho_L-\rho_g)\sigma]^{1/4}}\right)^{0.2}\left(\frac{V_{SG}^{2}}{gD}\right)^{0.18}$$

This transition boundary is plotted for the flow of R113 in a 0.4 mm microgap channel and 2 mm minigap channel in Figures 17 and 18, respectively. The area on the map shaded with light yellow represents the Intermittent to Annular regime transition according to Weisman et al. It is noticeable that the slope of this Weismann transition boundary is the opposite to the Taitel-Dukler Intermittent to Annular transition boundary and appears to capture a different phenomenological progression than the Taitel and Dukler map; transitioning from wavy Stratified behavior to Annular flow – as visible in the Ghajar (2006) empirical flow regime map - rather than from the Bubble and slug flow domains into Annular flow. Regrettably, much of the limited microgap refrigerant data currently available in the literature, including the Yang and Fujita (2004) and Lee and Lee (2001) data shown in Figures 17 and 18, respectively, clusters around the intersection of these two transition boundaries, making it difficult to judge the relative accuracy of these two distinct transition criteria.

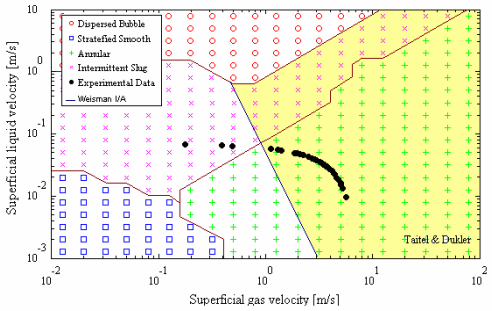

Figure 17: R113, Microgap, [Yang & Fujita (2004), R113, D_h = 0.396 mm, G = 100 kg/m^{2}s, q''= 20 kW/m^2]

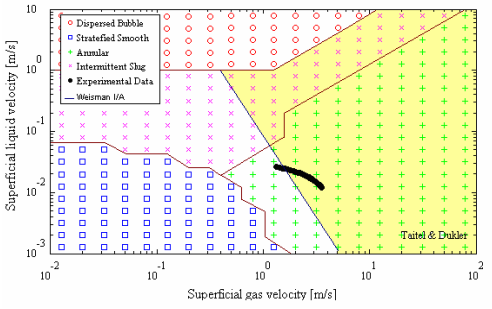

Figure 18: R113, Minichannel [Lee & Lee (2001), R113, D_h = 1.905 mm, G = 51 kg/m^{2}s, q''= 2.95 kW/m^2)

REVELLIN AND THOME DIABATIC FLOW REGIME MAP

Revellin and Thome (2006) proposed a new flow regime map for evaporating flow in microchannels. Their diabatic map classifies flows into three types: (a) The Isolated Bubble regime, (b) The Coalescing Bubble regime, and .(c) The Annular regime.

The Isolated Bubble regime is identified by having a bubble generation rate greater than the bubble coalescence rate, and includes both Bubble and slug flows. The vapor quality at which the maximum bubble frequency occurs marks the transition boundary from the Isolated Bubble regime to the Coalescing Bubble regime. The transition vapor quality was correlated By Revellin and Thome (2006) in terms of Webber number, Reynolds number, and the Boiling number, as:

$$x_{IB/CB} = 0.763\left(\frac{\mathrm{Re}_{LO}\ Bg}{We_{GO}}\right)^{0.41}$$

The Coalescing Bubble regime dominates when the bubble coalescence rate is much greater than the bubble generation rate. To correlate the transition from Coalescing Bubble regime to the Annular regime, Revellin and Thome gathered the vapor qualities that correspond to a bubble frequency of zero and proposed the following correlation that governs the transition boundary from Coalescing Bubble regime to Annular Regime:

$$x_{CB/A} = 0.00014\,\mathrm{Re}_{LO}^{1.47}\ We_{LO}^{-1.23}$$

The Annular regime is distinguished by the existence of thin liquid film and extents up to the critical heat flux limit at a relatively high vapor quality. A new version of Katto-Ohno (1984) CHF correlation was used to correlate the transition from Annular flow to Dryout, as proposed by Wojtan et al (2005).

$$q_{crit} = 0.437\left(\frac{\rho_V}{\rho_L}\right)^{0.073} We^{-0.24}\left(\frac{L}{D}\right)^{-0.72} G\ h_{LV}$$

The three transition boundaries are presented in Figure 19 (Revellin and Thome 2006)

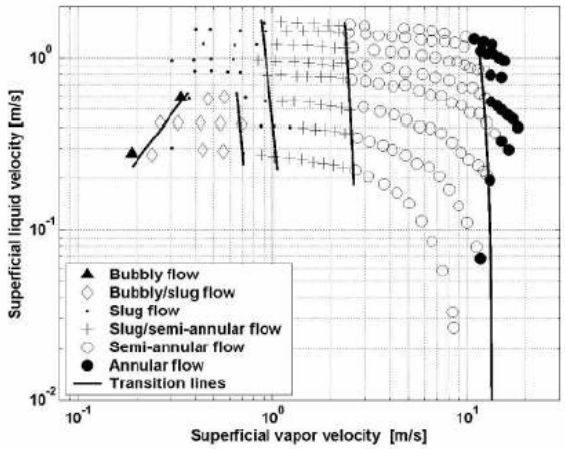

Figure 19: Revellin and Thome (2006) Diabatic Two-Phase Flow Regime Map.

SERIZAWA ET AL. OBSERVATIONS ON FLOW PATTERNS IN MICROCHANNELS

In their 2001 study of a 50 micron channel with steam-water flow, Serizawa et. al observed the progression in flow regimes from Bubble flow to Intermittent (slug) flow and into a unique flow regime – shown in Figure 20 - that they named "liquid ring" flow, before progressing into Annular (dispersed droplet) flow. In a 20 micron channel with air-water flow they observed the "liquid ring" behavior as well as another regime they named a "liquid lump flow".

Figure 20 Flow Visualization in Microchannels, Serizawa et. al (2001). Source: Thome (2006).

TABATABAI AND FAGHRI

In their 2001 paper, Tabatabai and Farghri proposed a new two-phase flow regime map to emphasize the importance of surface tension in two-phase flow in horizontal miniature passages. Using a force balance around an elongated bubble to determine when surface tension forces would exceed shear and buoyancy forces, they determined a criteria for the transition from surface tension dominated behavior to the shear-dominated behavior, as displayed on superficial velocity coordinates in the map of Figure 21. Since it is the Bubble and Intermittent regimes that can be expected to reflect the dominance of surface tension effects, in this map, as well as other maps for miniature passage configurations, it appears that this "new" regime combines large swaths of the Bubble and Intermittent regimes (with a smaller section of the Stratified domain) and occupies the upper left corner of the Taitel and Dukler flow regime map.

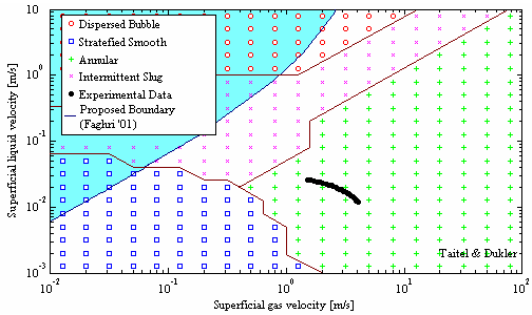

Figure 21: Tabatabai and Faghri Modified Flow Regime Map for R113, Mini-gap [Lee & Lee (2001), R113, D_h = 1.905 mm, G = 51 kg/m^{2}s, q''= 2.95 kW/m^2.

MICRO-CHANNEL DEFINITION

Mehendale et al (2000) considered the range from 1 micron to 100 micron as microchannels, 100 microns to 1 mm as mesochannels, 1 mm to 6 mm as compact passages, and greater than 6 mm as conventional passages. This classification was based merely on the dimension of the channel; fluid's properties are not taken into consideration.

Kandlikar and Grande (2003) considered conventional channels to be those with hydraulic diameter of 3 mm or larger. They considered the lower limit for manufacturing smaller channels to be imposed by the major changes in fabrication technology, warranted below 200 microns. Hence, they considered channels with a hydraulic diameter range of 200 micron to 3 mm to be classified as minichannels.
They considered the range below 200 microns which they called "microchannels" to be influenced by the rarefaction effects for gases described by the Knudsen number as :

$$Kn = \frac{\lambda}{Dh} \quad , \quad \lambda = \frac{\mu\sqrt{\pi}}{\rho\sqrt{2RT}}$$

where lambda is the mean free path for the gas and R being the gas constant. The range between 10 micron and 200 micron is generally affected by the rarefaction effects for many gases, and approximately corresponds to the Knudsen number values of 0.001 to 0.1 for various cryogenic gases.
Rarefaction effects are more severe in the region between 10 micron and 0.1 micron, and this is referred to as the transitional region, that yields Knudsen numbers of the values 0.1 to 10 for several cryogenic gases as well.

Kandlikar and Grande suggested these criteria that were developed from gas flow consideration, yet they recommended the same considerations for both liquid and two-phase flow applications as well in order to obtain a uniform channels classification.

Conventional channels:	D_h>3 mm
Minichannels:	3mm >= D_h >200 micron
Microchannels:	200 micron >= D_h > 10 micron
Transitional channels	10 micron >= Dh > 0.1 micron
Transitional microchannels	10 microns >= Dh > 1 micron
Transitional nanochannels	1 micron >= Dh > 0.1 micron
Molecular nanochannels	0.1 microns >= Dh

However, when applying the above criteria to water and Freon R113 it was found that the micro region being identified with Knudsen numbers of 0.001 to 0.1 yields values of 305 to 3 microns for water, and 2 micron to 0.02 micron for Freon R113 when using the gas properties. Diameters values were significantly smaller when applying the liquid properties.

Kew & Cornwell (1997) adopted a different method to what constitutes a micro-channel. Based on the definition of the confinement number, introduced by the authors, as:

$$Co = \frac{[\sigma/(g(\rho_L - \rho_v))]^{1/2}}{d}$$

They performed a statistical comparison of the prediction of the following two phase heat transfer correlations:

Liu and Winterton (1988), Cooper (1984), Cooper (1989), Lazarek and Black (1982), Modified Lazarek and Black (1982) and Tran et al (1995) to the measured data of about 700 points. They found the subset of the data which has a confinement number values of below 0.5 to be in a better agreement with the conventional correlation than the subset with confinement number values greater than 0.5. The results of Kew and Cornwell (1997) statistical results are listed in Table 3

Table 3: Statistical Comparison by Kew and Cornwell (1997)

Tube Descreption [mm]	3.69	2.87	2.05	1.39	2.10*	2.92
Co	0.33	0.42	0.59	0.87	0.57	0.34
Number of Points	146	141	182	79	149	
Liu and Winterton (1988)	21	42	118	259	72	15
Cooper (1984)	25	21	30	36	33	
Cooper (1989)	36	46	43	69	54	
Lazarek and Black (1982)	22	19	47	69	39	
Modified Lazarek and Black (1982)	23	19	48	71	39	
Tran et al. (1995)	24.9	32.7	37.3	39.3		

* Square Channel.

Figure 22 illustrates the micro- and mini-channels convention according to Mehendale et al, Kandlikar & Grande, and Kew & Cornwell.

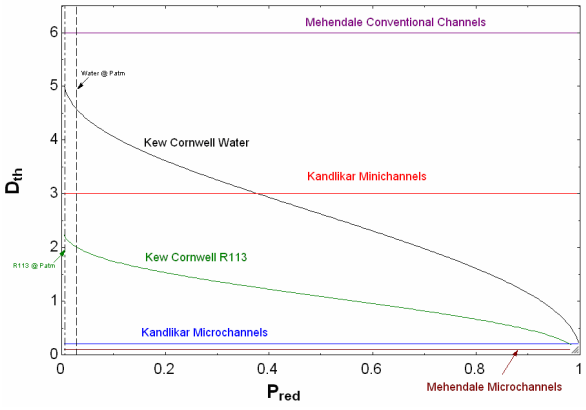

Figure 22: Different convention for small channels.

LITERATURE REVIEW AND DATA BASE DESCRIPTION

To evaluate the efficacy of using a flow-regime-informed approach to the prediction and correlation of two-phase microchannel and microgap cooler behavior an extensive set of experimental studies of two-phase mini- and micro-channel heat transfer and fluid mechanics behavior was identified and is listed in Table 3. The available data is seen to span a broad range of parameters, geometries, and working fluids. The hydraulic diameter ranges from 100 micron to 3.6 mm, the heat flux is up to 2058 kW/m^2, and the mass flux ranges from 52 kg/m^{2}s to 1782 kg/m^{2}s. The fluids are Refrigerants Freon R21 and Freon R113, Vertrel XF ™, HFE-7100 ™, n-Octane, n-Hexane, and water. Channel geometries vary between triangular, rectangular typical multi-ports channels to single gap with aspect ratios that reaches as high as 1/100. Some of the more prominent studies in this database are reviewed below, and a sample of flow regime maps for several of the channel geometries, hydraulic diameters, and working fluids, is shown, along with the empirical axial variation in the heat transfer coefficients plotted against the superficial gas velocity or fluid quality in the channel.

In their study, Steinke and Kandlikar (2004) reported experiments on water flowing in 6 parallel horizontal rectangular channels of a hydraulic diameter of 207 micron. They measured wall temperatures using 6 thermocouples along the 57 mm long channel. In the analysis of their 241 data points, Steinke and Kandlikar used a decreasing saturation temperature along the channel, based on an assumed linear axial variation of pressure. The total pressure drop was measured experimentally and reached up to 76 kPa. They observed the Annular flow to be one of the dominant flow regimes along with the elongated bubble regime. Figure 23 shows Taitel-Dukler flow regime map for Steinke and Kandlikar data.

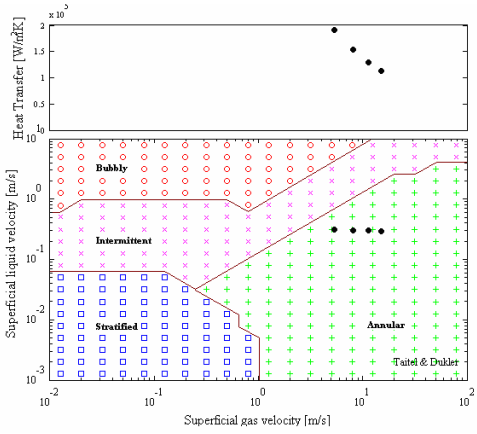

Figure 23: Taitel-Dukler flow regime map [Steinke and Kandlikar (2004), Water, Dh=0.207 mm, G=1782 kg/m^{2}s, q"=643 kW/m^2).

Madrid et al. (2006) used HFE7100 in 40 parallel vertical rectangular channels 220 mm long with a hydraulic diameter of 0.840 mm. A set of five thermocouples was used to determine the channel wall temperature. The pressure was

measured at the inlet and outlet of the channel, and the homogeneous two-phase pressure drop model was used to estimate the local pressure values along the channel. The fluid saturation temperature therefore was found from the pressure profile.
For their 258 data points, the mass flux ranges from 71 to 191 kg/m^{2}s, and the heat flux from 1.7 to 4.6 kW/m^2 and the heat transfer coefficient reaches as high as 5700 W/m^{2}K.

They observed the heat transfer coefficient to have almost a constant flat value at a low vapor quality, where dominant flow regime could be the Bubble or Intermittent flow regime, then the heat transfer coefficient increases at higher quality where Annular flow regime dominates, before it drops drastically at a further higher quality where dryout occurs. Figure 24 shows the agreement between Madrid et al. observation on flow regime and Taitel-Dukler flow regime map for the case of mass flux = 97 kg/m^{2}s and heat flux of 2.3 kW/m^2.

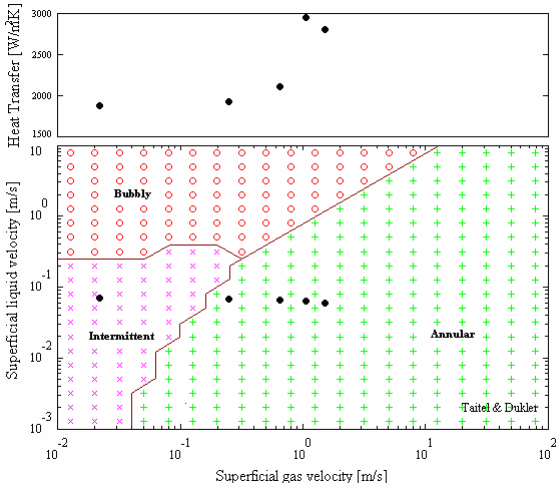

Figure 24: Taitel-Dukler map for Madrid et al. (2004), HFE7100, Dh=0.840 mm, G=97 kg/m^{2}s, q'' = 2.3 kW/m^2.

Phase change heat transfer in parallel plate micro-gaps was investigated by several researchers. Lee and Lee (2001) used R113 in a 300 mm long single horizontal rectangular gap. Hydraulic diameter varied from 0.396 – 3.636 mm. Seven thermocouples were used to measure wall temperature along the channel. For their 491 data points, they accounted for variable saturation temperatures along the channel with respect to a model-predicted pressure variation along the channel. The total pressure drop was measured experimentally, and reached up to 40 kPa. Lee and Lee (2001) observed the Annular flow to dominate , which agrees very well with the flow regime map generated for this study as shown in Figure 25 generated for R113 flowing in 0.4 mm height gap.

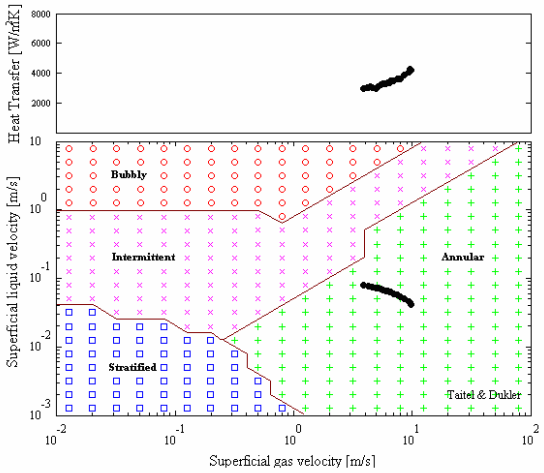

Figure25: Taitel-Dukler Flow Regime Map for 0.4 mm Refrigerant Microgap Channel [Lee & Lee (2001), R113, G=155 kg/m^{2}s, q''=5 kw/m^2, D_h= 784 micron single channel.]

Yang and Fujita (2004) used R113 in a very similar experimental setup; 100mm long single horizontal rectangular gap, with the width fixed at 20mm while the height varied from 0.2 to 2 mm to yield hydraulic diameters from 0.396 to 3.636 mm. Five pairs of thermocouples were used to determine the wall temperature and the heat flux. In their database of 292 points, the mass flux varies from 50 to 200 kg/m^{2}s and the heat flux from 20 to 90 kW/m^2.

The flow regime map and heat transfer coefficient variation for a typical configuration (0.5mm gap) in the Yang and Fujita mini-gap channel (2004) is displayed in Figure 26. The authors observed Intermittent flow at the lower vapor quality and Annular flow regime occupying the region of vapor quality higher than 0.2 with a decided absence of Bubble flow. This observation agrees with the flow regime map generated for the average channel pressure, as previously discussed.

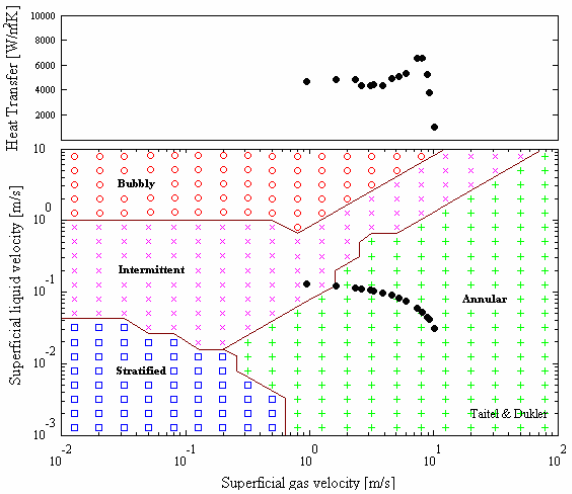

Figure 26 : Taitel-Dukler Flow Regime Map for 0.5 mm Refrigerant Microgap Channel [Yang & Fujita (2004), R113, G=200 kg/m2s, q''=50 kw/m2, Dh= 976 micron single channel]

Kuznetsov and Shamirzaev (2006) used R21 in a single vertical channel with dimension of 1.6 by 6.3 mm that yields a hydraulic diameter of 2.552 mm. Four thermocouples were used along the channel length of 290 mm. The heat transfer coefficient was calculated based on saturation temperature at each site, assuming that the pressure varied linearly between the inlet and outlet of the channel. They reported the dominance of convective boiling even at low fluid quality, and steeper increases in the heat transfer coefficient at qualities greater than 0.5, where heat transfer behavior seemed to be dominated by thin film evaporation.

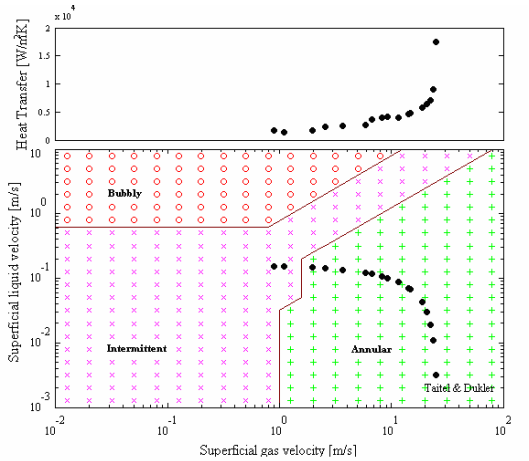

Figure 27: Taitel-Dukler flow regime map for data of Kuznetsov and Shamirzaev (2006), R21, D_h= 2.552 mm, G=215 kg/m^{2}s, q''= 6 kW/m^2.

Cortina-Diaz and Schmidt (2006) investigate flow boiling heat transfer in a single vertical channel. They used n-Hexane and n-Octane in a single 12.7 by 0.3 mm channel with a hydraulic diameter of 0.586 mm. Infrared thermography was employed to measure the channel surface temperature. A linear axial pressure variation in the channel was assumed from onset of flow boiling and within the two-phase flow region. From Figure[] it can be observed that a change in the trend of heat transfer coefficient can be observed in the proximity of flow regime transition boundary from Intermittent into Annular. Once into the Annular flow, the heat transfer coefficient keeps increasing until it reaches a local peaks after which it changes slope and drops drastically till the end of the channel, as shown in Figure 28.

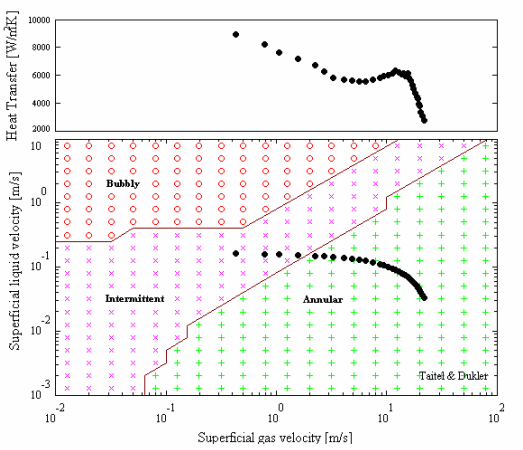

Figure 28: Taitel-Dukler flow regime map for data of Cortina-Diaz and Schkidt (2006), n-Octane, D_h= 0.586 mm, G=100 kg/m^{2}s, q''= 37.8 kW/m^2.

Huh and Kim (2006) used deionized water in a single horizontal rectangular channel with a hydraulic diameter of 0.1 mm and length of 40 mm. The mass flux ranged from 90 to 267 kg/m^{2}s and the heat flux from 100 to 600 kW/m^2. Using a high speed CCD camera with microscope, they observed the major flow pattern to be Annular flow, which agrees with prediction of Taitel and Dukler methodology as shown in Figure29

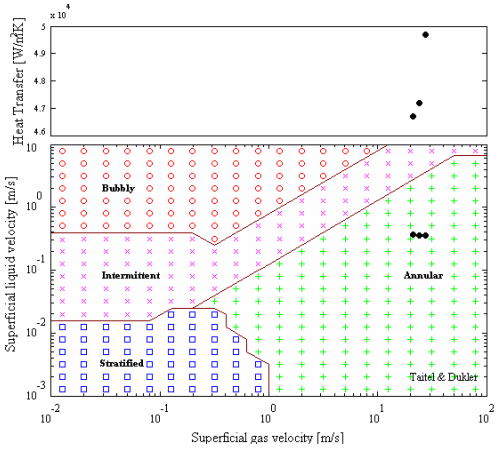

Figure 29: Taitel-Dukler flow regime map for data of Cortina-Diaz and Schkidt (2006), n-Octane, D_h= 0.586 mm, G=100 kg/m^{2}s, q''= 37.8 kW/m^2.

From a total of 2259 two-phase points gathered from the open literature for this study, approximately 2/3rds, or 1586, were obtained from flows in mini- and microgaps, while 1/3 rd or 673 data points were extracted from experiments with multiple channel mini-and microchannel coolers. Most of the data points fell in the Annular flow regime when sorted according to Taitel and Dukler flow regime maps; 1994 points fell into the Annular flow regime while 265 points fell into the Intermittent flow regime. The studies from which the database points are gathered are listed in Table 4.

Table 4: Two-Phase Literature Review.

Author	Year	Fluid	Test Section	Dh [mm]	q'' [kW/m^2]	G [kg/m^{2}s]	Pressure [kPa]	Number of Points	x
Ravigururajan	1999	R124	54 rectangular channels	0.425	54.1-631	138-399	445	30	0.02-0.85
Lee & Lee	2001	R113	Single gap 2x20, 1x20, and 0.4x20	3.636, 1.905, 0.784	3-15	52-208	108-128	481	0.18-0.76
Hetsroni et al	2002	Vertrel XF	21 triangular channels	0.130	22.4-59	148-290	101.3	12	0.03-0.18
Qu & Mudawar	2003	Water	21 Rectangular Channels	0.349	213-2058	135-400	117-200	184	0.01-0.17
Yang & Fujita	2004	R113	Single gap 2x20, 1x20, 0.5x20, and 0.2x20	3.636, 1.905, 0.976, 0.396	20-90	100-200	101-219	292	0.01-0.96
Kuwahara et al	2004	R134a	8 rectangular channels	1.06	30	204-607	500	20	0.19-0.67
Steinke & Kandlikar	2004	Water	6 rectangular channels	0.207	55-898	157-1782	125-202	169	ɔoled-0.959
Madrid et. al.	2006	HFE 7100	40 vertical rectangular channels	0.840	1.7-4.6	71-191	101.3	259	0-0.94
Cortina-Diaz & Schmidt	2006	n-hexane, n-octane	Single vertical rectangular channel	0.586	11.6-148.3	100-400	101.3	724	Subcooled -0.8
Huh & Kim	2006	water	Single rectangular channel	0.100	223-506	90-363	101-139	31	0.04-0.37
Sobierska et. al.	2006	Water	Single Vertical rectangular channel	0.480	35-196	200-1500	60-120	67	Subcooled -0.27
Kuzentsov & Shamirzaev	2006	R21	Single vertical rectangular Channel	2.552	6	215	194	17	0.04-0.98

VARIATION AND COMPARISON OF HEAT TRANSFER COEFFICIENTS

Figure 30 displays the axial variation in the heat transfer coefficient and reveal the existence of a characteristic curve, which is visible in its entirety in about half of the cases studied. The characteristics axial variation of the heat transfer coefficient, as may be best seen in Figures 30, 24 and 28, displays two inflection points – the first corresponding approximately to the Intermittent to Annular flow transition and the second occurring deep in the annular regime. The first inflection point, occurring where vapor slug heat transfer gives way to thin film evaporation, begins the transition to elevated values of the heat transfer coefficient. The second inflection point, corresponding to the maximum heat transfer coefficient, occurs at still moderate qualities which are often lower than dry-out or CHF values predicted by the available CHF correlations; a comparison between the vapor quality at the second inflection point and that predicted by Biasi (1967), Bowring (1972), Levitan & Lantsman (1972), Qu & Mudawar (2004), and Wojtan et al. (2005) CHF correlations proved that the second inflection point in the heat transfer coefficient locus occur at a vapor quality consistently smaller than the CHF predicted vapor quality. In addition, the axial heat transfer coefficient at qualities greater than those at the second inflection point decrease at a gradual rather than precipitous rate as might have been expected had traditional dry-out occurred. Therefore, it is suggested that microgap channels experience an extended dryout sub-regime, whose onset has yet to be determined. Other studies which do not show the full characteristic curve, appear to partially reflect this characteristic axial variation namely, the low quality annular regime alone or the extended dryout sub-regime alone.

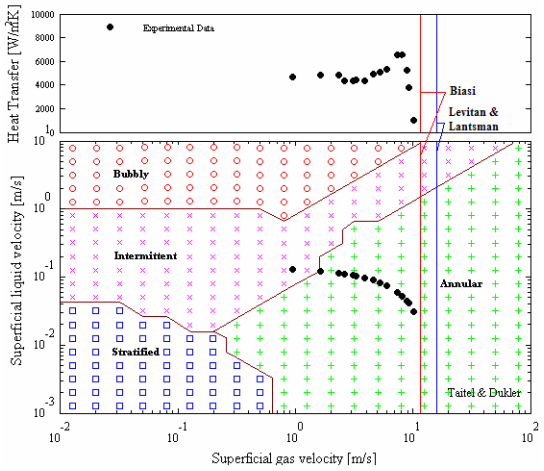

Fig 30 : Taitel-Dukler Flow Regime Map for 0.5 mm Refrigerant Microgap Channel [Yang & Fujita, R113, G=200 kg/m^{2}s, q''=50 kw/m^2, D_h= 976 micron single channel.]

AXIAL VARIATION OF HEAT TRANSFER COEFFICIENTS

Figure 30 which displays the thermofluid data for the 0.5mm minigap channel studied by Yang and Fujita (2004), it may be seen that plotting the heat transfer coefficient against the superficial gas velocity, reveals the existence of a characteristic axial variation in the two-phase heat transfer coefficient. The heat transfer coefficient is found to be nearly constant in the low quality Intermittent regime, to rise steeply as transition is made to moderate quality Annular flow (at a quality of 0.125), reaching a peak value at a quality of 0.567 before falling precipitously as complete evaporation (100% quality) is approached.

This behavior can be understood to reflect the underlying thermo-physics of two-phase thermal transport in mini-channels. Heat transfer coefficients increase with transition from Intermittent (slug/plug) flow to annular flow, where thin film evaporation begins to dominate, and continue to increase in the annular regime due to thinning of the evaporating film. Deep into the annular regime, but prior to the experimentally observed dryout limit, a decrease in heat transfer coefficient occurs, possibly due to partial dryout of the liquid film.

COMPARISON TO CLASSICAL CORRELATIONS

In evaluating and comparing these heat transfer coefficients to the available correlations, the data was divided into three categories: Intermittent Flow, Annular Flow-low quality, and Annular Flow – high quality. The peak heat transfer coefficient for each case was used as the criteria for separating the "low quality" and "high quality" sub-regimes of annular flow. It is also to be noted that in this analysis, the local channel pressure (for determination of fluid properties and gas velocities) was evaluated by the method described in each of the selected studies. The Hydraulic diameter for the two-phase heat transfer comparison purposes was defined as:

$$D_h = \frac{4\times(Channel Cross sectional Area)}{Heated Perimeter}$$

Applying the procedure mentioned above, a statistical analysis was performed to determine the discrepancy between the aforementioned classical two-phase heat transfer correlations and the mini- and micro-channel heat transfer data in the selected studies listed in Table 4. The relative error in prediction of heat transfer coefficient was calculated as:

$$\varepsilon_i = \frac{\left|h_{predicted} - h_{measured}\right|}{h_{measured}}$$

The average error for a set of data was calculated as:

$$\varepsilon_{average} = \sum_i^n \frac{\varepsilon_i}{n}$$

Two additional criteria were used to compare the data discrepancy with correlations. The Normalized RMS used here is defined as:

$$\varepsilon_{RMS} = \sqrt{\sum_{i=1}^{n} \frac{\varepsilon_i^2}{n}}$$

And the standard deviation used is defined as:

$$\sigma = \sqrt{\sum_{i=1}^{n} \frac{\left(\varepsilon_i - \varepsilon_{AVE}\right)^2}{n}}$$

Additionally, the statistical analysis attempted to determine the extent to which the prevailing flow regime and/or the domain of the annular flow regime, i.e. low quality or high quality, can influence the accuracy of these correlations.

Table 5 provides a summary of the average discrepancy between the selected correlations, (appendix a – e), and the examined dataset of 2259 data points, in the different regimes. As previously noted the vast majority of the data considered in this study was found to be in the annular regime, as also generally observed by the respective researchers and supported by the flow regime mappings for the specific flows and channel geometries considered.

The data was classified based on the channel configuration; single gap or multi-channels, and the operating fluid being water or refrigerants. The data of Cortina-Diaz and Schmidt (2006) of n-octane and n-hexane was combined with the water data.

Table5: Discrepancy of Two-Phase data classified by working fluid and channel configuration. (%)

Geometry		Gaps		Channels	
Fluid		Dielectric Liquids	Water, n-Octane, n-Hexane	Dielectric Liquids	Water
Number of Data Points		790	796	320	353
Chen	ε_{AVE}	28	66	55	95
	σ	26	69	125	118
	ε_{RMS}	38	95	137	136
Kandlikar	ε_{AVE}	55	54	52	67
	σ	25	54	86	67
	ε_{RMS}	61	76	101	94
Gungor-Winterton	ε_{AVE}	39	102	89	160
	σ	49	80	180	117
	ε_{RMS}	63	130	201	198
Gungor-Winterton Revised	ε_{AVE}	34	72	63	102
	σ	23	67	131	80
	ε_{RMS}	41	99	146	130
Shah	ε_{AVE}	39	68	57	104
	σ	13	65	140	88
	ε_{RMS}	41	94	151	137

As may be seen in Table 5, the discrepancy between the classical correlations and the data points varies depending on the channel configuration and operating fluid, with data of refrigerants in single gap channel having a better agreement with the classical correlations. One main reason could be the flow instability among other phenomena known to occur in multichannel configurations (Bergles and Kandlikar, 2005)

Alternatively, when the single gap data with refrigerants as operating fluids is divided between the intermittent, low-quality and the high-quality domains of the annular regime, it is seen that very large discrepancies are encountered with the high-quality data, while surprisingly good agreement, in the range of an average discrepancy of 24% to 36%, is attained with the data points that fall in the low-quality domain, namely with Chen, Gungor-Winterton revised, and Shah correlations, as Shown in Table 6.

Table 6: Discrepancy between two-phase refrigerants data in single gap channels and conventional correlations. (%)

Regime		Inter-mittent	Annular-Low Quality	Annular-High Quality
Number of Data Points		44	687	59
Chen	ε_{AVE}	72	24	39
	σ	20	20	51
	ε_{RMS}	75	31	64
Kandlikar	ε_{AVE}	36	57	48
	σ	25	25	22
	ε_{RMS}	44	62	52
Gungor-Winterton	ε_{AVE}	72	36	54
	σ	46	45	75
	ε_{RMS}	85	58	92
Gungor-Winterton Revised	ε_{AVE}	34	33	37
	σ	25	21	36
	ε_{RMS}	42	40	52
Shah	ε_{AVE}	32	32	40
	σ	23	22	44
	ε_{RMS}	40	39	59

CONCLUSIONS

A careful reading of the available literature reveals a strong dependence of thermal transport phenomena in tubes and channels on the prevailing flow regimes. A detailed analysis of microchannel/microgap heat transfer data for two-phase flow of refrigerants and dielectric liquids, gathered from the open literature and sorted by the Taitel and Dukler flow regime mapping methodology, reveals that approximately 90% of the more than 2000 data points fell in the Annular flow regime and the other 10 % in the intermittent regime, in strong agreement with the reported observations. The dominance of the Annular flow regime is seen to grow with decreasing channel diameter and may well serve to define the transition from macro- to microchannel behavior.

A characteristic axial heat transfer coefficient curve in microgap channels has been identified, displaying strongly increasing values following the transition from the Intermittent into low-quality Annular flow and a steeply decreasing locus following the onset of partial dryout at higher vapor qualities. Comparison of the microgap data to existing correlations, revealed that the dominant, axially-increasing low quality Annular data could be correlated by the Chen correlation to

within an average discrepancy of 24%, while the Shah correlation provided agreement to within an average discrepancy of 32% for data in the Intermittent regime, and the modified Gungor-Winterton correlation approximately 37% for the moderate-quality annular flow data. The transition from the low-quality to moderate-quality behavior was found to occur at qualities well below predicted dryout or CHF values and appears to be associated with the onset of local dryout in the channel.

ACKNOWLEDGMENTS

This effort has been supported by the Office of Naval Research. The authors thank Dr. Mark Spector for his guidance and useful discussions of this work.

REFERENCES

Baker, O., 1954, "Simultaneous Flow of Oil and Gas," Oil and Gas J., 53 (12), 185-195.

Bar-Cohen, A., Ruder, Z., and Griffith, P., 1987, "Thermal and Hydrodynamic Phenomena in a Horizontal Uniformly Heated Steam Generating Pipe," Journal of Heat Transfer, 109, 739-745.

Bar-Cohen, A., Sherwood, G., Hodes, M., and Solbrekken, G., 1995, "Gas-Assisted Evaporative Cooling of High Density Electronic Modules," IEEE Transactions on Components, Hybrids, and Manufacturing Technology, 18 (3), 502-509.

Bar-Cohen, A., Bergles, A. E., and Pribyl, D., 2005, "Relating Critical Heat Flux to the Two-Phase Flow Regimes in Upward Steam and Water Flow," Invited Lecture, XV Seminar – School, Problems of Gas Dynamics, Heat and Mass Transfer in Power Plants," Kaluga, Russia, May 23-27.

Benjamin, T.B., 1968, "Gravity Currents and Related Phenomena," J. Fluid Mech., 31, 209-248.

Bergles, A.E., and Kandlikar, S.G., 2005, "On the Nature of Critical Heat Flux in Microchannels," Journal of Heat Transfer (125), 101-107.

Biasi, L., et al., 1967, "Studies on Burnout, Part 3." Energia Nucleare. 14 (9), 530-536.

Bowring, R.W., 1972, "A simple but accurate round tube uniform heat flux, dryout correlation over the pressure range 0.17-17 MN/m^2 (100-2500 psia)." AEEW-R, 789.

Chen, J.C., 1966, "Correlation for boiling heat transfer to saturated fluids in convective flow, Industrial and Engineering Chemistry," Process Design and Development, 5 (3), 322-329.

Chisholm, D., 1973, "Pressure Gradient Due to Friction During the Flow of Evaporating Two-Phase Mixtures in Smooth Tubes and Channels," Int. J. Heat Mass Transfer, 16, 347-357.

Cooper, M.G., 1984, "Saturated Nucleate Pool Boiling – a Simple Correlation." 1st UK National Heat Transfer Conference. IChemE Symp. Series No. 86 (2), 785-793.

Cooper, M.G., 1989, "Flow Boiling – the Apparently Nucleate Regime," Int. J. Heat Mass Transfer, 32, 459-464.

Frankum, D.P., Wadekar, V.V., and Azzopardi, B.J., 1997, "Two-phase flow patterns for evaporating flow," Experimental Thermal and Fluid Science, 15, 183-192.

Cortina-Diaz, M., and Schmidt, J., 2006, "Flow Boiling Heat Transfer of n-Hexane and n-Octane in a Minichannel," . Proceedings of the 13th International Heat Transfer Conference, Sydney, Australia.

Ghajar, A., Kim, A.J., and Tang, C., 2006, "Two-Phase Flow Heat Transfer Measurements and Correlation for the Entire Flow Map in Horizontal Pipes," Proceedings of the 13th International Heat Transfer Conference, Sydney, Australia.

Gungor, K.E., and Winterton, R.H.S., 1986, "A General Correlation for Flow Boiling in Tubes and Annuli," Int/ J. Heat Mass Transfer, Vol. 29, No. 3, 351-358.

Gungor, K.E., and Winterton, R.H.S., 1987, "Simplified General Correlation for Saturated Flow Boiling and Comparisons of Correlations with Cata," Chemical Engineering Research and Design, 65, 148-156.

Hetsroni, G., 1982, Handbook of Multiphase Systems, Hemisphere Publishing Co.

Hetsroni, G., Mosyak, A., Segal, Z., Ziskind, G., 2002, "A Uniform Temperature Heat Sink For Cooling of Electronic Devices," Int. J. Heat Mass Transfer, 45, 3275-3286.

Huh, C., Kim, M.H., 2006, "Two-Phase Pressure Drop and Boiling Heat Transfer in a Sinlge Horisontal Microchannel," Proceedings of the 4th International Conference on Nanochannels, Microchannels, and Minichannels, Limerick, Ireland.

Kandlikar, S.G. and Grande, W.J., 2003, "Evolution of Microchannel Flow Passages – Thermohydraulic Performance and Fabrication Technology," Heat Transfer Engineering, 24(1), 3-17.

Kandlikar, S.G. and Balasubramanian, P., 2004, "An extension of the flow boiling correlation to transition, laminar, and deep laminar flows in minichannels and microchannels," Heat Transfer Engineering, 25 (3), 86-93.

Katto Y. and Ohno H., 1984, "An Improved Version of The Generalized Correlation of Critical Heat Flux for the Forced Convective Boiling in Uniformly Heated Vertical Tubes," J. Heat and Mass Transfer. 9(9), 1641-1648.

Kew, P.A. and Cornwell, K., 1997, "Correlations for the Prediction of Boiling Heat Transfer in Small-Diameter Channels. Applied Thermal Engineering, 17(8-10), 705-715.

Kim H.G. and Lee, J.C., 1997, "Development of a Generalized Critical Heat Flux Correlation Through The Alternating Condition Expectation Algorithm," Nuclear Science and Engineering. 127, 300-316.

Kuwahara, K., Koyama, S. and Kazari, K., 2004, "Experimental study on flow boiling of HFC134a in a multi-port extruded tube," 2nd International Conference on Microchannels and Minichannels, New York, USA.

Kuznetsov, V.V. and Shamirzaev, A.S., 2006, "Boiling Heat Transfer for Freon R21 in Rectangular Minichannel," Proceedings of the 4th International Conference on Nanochannels, Microchannels, and Minichannels, Limerick, Ireland.

Lazarek, G.M., Black, S.H., 1982, "Evaporative Heat Transfer, Pressure Drop, and Critical Heat Flux in a Small Vertical Tube with R113," Int. J. Heat Mass Transfer. 25(7), 945-960.

Lee, H.J. and Lee, S.Y., 2001, "Heat Transfer Correlation for Boiling Flows in Small Rectangular Horizontal Channels with Low Aspect Ratios," Int. J. Multiphase Flow, 27, 2043-2062.

Levitan, L.L. and Lantsman, F.P., 1972, "Investigating Burnout with Flow of a Steam-Water Mixture in a Round Tube", Thermal Eng. (USSR), English Transl., 19 (3), 105-107.

Lin, S., Kew, P.A. and Cornwell, K., 2001, "Two Phase Heat Transfer to a Refrigerant in a 1mm Diameter Tube," Int. J. Refrig. 24, 51-56.

Liu, Z. and Winterton, R.H.S., A, 1991, "General Correlation for Saturated and Subcooled Flow Boiling in Tubes and Annuli Based on a Nucleate Boiling Equation," Int. J. Heat Mass Transfer, 34(11), 2759-2766.

Madrid, F., Caney, N. and Marty, P., 2006, "Flow Boiling Study in Mini-Channels," Proceedings of the 4th International Conference on Nanochannels, Microchannels, and Minichannels, Limerick, Ireland.

Mandhane, J.M., Gregory, G.A. and Aziz, K., 1974, "A Flow Pattern Map for Gas Liquid Flow in Horizontal Pipes," Int. J. Multiphase Flow, 1, 534-553.

Martinelli, R.C., Nelson, D. B., 1948, "Prediction of Pressure Drop during Forced-Circulation Boiling Water," Trans. ASME, 70, 695-702.

Mehendale, S.S., Jacobi, A.M.and Shah, R.K., 2000, "Fluid Flow and Heat Transfer at Micro- and Meso-Scales with Applications to Heat Exchanger Design," Applied Mechanics Review, 53, 175-193

Momoki, S., Bar-Cohen, A, and Bergles, A.E., 2000, "Estimation of Major Correlations for Frictional Pressure Drop in Gas-Liquid Two-Phase flow in Horizontal Pipes Using Predicted Flow Regime Information," Multiphase Science and Technology. 12 (3-4), pp 161-175.

Qu, W. and Mudawar, I., 2003, "Flow boiling heat transfer in two-phase micro-channel heat sinks—II Annular two-phase flow model," Int. J. Heat Mass Transfer, 46, 2773-2784.

Qu, W. and Mudawar, I., 2004, "Measurement and Correlation of Critical Heat Flux in Two-Phase Micro-Channel Hat Sinks," Int. J. Heat Mass Transfer, 47, 2045–2059.

Ravigururajan, T.S., 1999, "Two-Phase Flow Characteristics of Refrigerant Flows in a Microchannel Heat Exchanger," Enhanced Heat Transfer, 6, 419-427.

Revellin, R., Thome, J.R., 2006, "New Diabatic Flow Pattern Map for Evaporating Flows in Microchannels," Proceedings of the 13th International Heat Transfer Conference, Sydney, Australia.

Serizawa, A., Feng, Z.P., 2001, "Two-Phase Flow in Microchannels," International Conference of Multiphase Flows, New Orleans, Keynote Lecture.

Shah, M.M., 1976, "A New Correlation for Heat Transfer During Boiling Flow Through Pipes, ASHRAE Transactions, 82 (2), 66-86.

Shoham, O., 1982, "Flow Pattern Transition and Characterization in Gas-Liquid Flow in Inclined Pipes," PhD. Dissertation, Tel-Aviv University, Ramat-Aviv, Israel.

Sieder, E.N. and Tate, G.E., 1936, "Heat Transfer and Pressure Drop of Liquids in Tubes," Industrial and Engineering Chemistry, Vol 28, No. 12, PP 1429-1435

Simpson, H.C., Rooney, D.H., Gratton, E., and Al-Samarral, F., 1997, "Two-Phase Flow in Large Diameter Horizontal Lines," Paper H6, European Two-Phase Flow Group Meeting, Grenoble.

Sobierska, E., Kulenovic, R., and Mertz, R., 2006, "Heat Transfer Meachanism and Flow Pattern During Flow Boiling of Water in a Vertical Narrow Channel – Experimental Results," Proceedings of the 4th International Conference on Nanochannels, Microchannels, and Minichannels, Limerick, Ireland.

Steinke, M., and Kandlikar, S.G., 2004, "An Experimental Investigation of Flow Boiling Characteristics of Water in Parallel Microchannels," ASME Journal of Heat Transfer, 126, 518-526.

Tabatabai, A., and Faghri, A., 2001, "A New Two-Phase Flow Map and Transition Boundary Accounting for Surface Tension Effects in Horizontal Miniature and Micro Tubes," Journal of Heat Transfer, v 123, n 5, p 958-968

Taitel, Y., and Dukler, A.E., 1976, "A Model For Predicting Flow Regime Transitions in Horizontal and Near Horizontal Gas-Liquid Flow", AIChE Journal, 22 (1), 47-55.

Taitel, Y., and Dukler, A.E., 1987, "Effect of Pipe Length on the Transition Boundaries for High Viscosity Liquids," Int. J. Multiphase Flow, Vol. 13, pp 577-581.

Taitel, Y., 1990, "Flow Pattern Transition in Two Phase Flow," Keynote, Proceedings of the 9th International Heat Transfer Conference, Jerusalem, Israel, 237-254.

Thom, J. R. S., 1964, "Prediction of Pressure Drop during Forced Circulation Boiling of Water," Int. J. Heat. Mass Transfer, 7, 709-724.

Thome, J.R., 2006, "Fundamentals of Boiling and Two-Phase Flow in Microchannels," Keynote, Proceedings of the 13th International Heat Transfer Conference, Sydney, Australia.

Tran, T.N., Wambsganss, M.W., and France, D.M., 1995, "Boiling Heat Transfer with Three Fluids in Small Circular and Rectangular Channels," Argonne National Laboratory, Report ANL-95-9. NTIS, Springfield, VA.

Weisman, J., Duncan, D., Gibson, J., and Crawford, T., 1979, "Effect of Fluid Properties and Pipe Diameter on Two-Phase Flow Pattern in Horizontal Lines," Int. J. Multiphase Flow, 5, 437-462.

Wojtan, L., Revellin, R., and Thome, J.R., 2005, "Investigation of Critical Heat Flux in Single, Uniformly Heated Microchannels," ECI International Conference on Heat Transfer and Fluid Flow in Microscale, Castelvecchio Pascoli, 25-30 Sept.

Yang, Y., and Fujita, Y., 2004, "Flow Boiling Heat Transfer and Flow Pattern in Rectangular Channel of Mini-Gap," 2nd International Conference on Microchannels and Minichannels (ICMM2004-2383), New York, USA.

APPENDIX: HEAT TRANSFER CORRELATIONS

A) CHEN CORRELATION (1966)

The starting point for the Chen correlation is:

$$h = h_{mic} + h_{mac}$$

The macroscopic contribution was calculated using the Dengler Addoms correlation with a Prandtl number correction factor to generalize the correlation beyond water as the working fluid.

$$h_{mac} = h_l F(X_{tt}) \mathrm{Pr}_l^{0.296}$$

Here the single phase liquid only convective coefficient (hl) is calculated via the Dittus-Boelter equation:

$$h_l = 0.023 \left(\frac{k_l}{D} \right) \mathrm{Re}_l^{0.8} \mathrm{Pr}_l^{0.4}$$

where: $\mathrm{Re}_l = \frac{G(1-x)D}{\mu_l}$. The microscopic contribution was calculated using the Forster-Zuber correlation for pool boiling with an additional correction factor in the form of a suppression factor:

$$h_{mic} = 0.00122 \left[\frac{k_l^{0.79} c_{pl}^{0.45} \rho_l^{0.49}}{\sigma^{0.5} \mu_l^{0.29} h_{lv}^{0.24} \rho_v^{0.24}} \right] [T_w - T_{sat}(P_l)]^{0.24} [P_{sat}(T_w) - P_l]^{0.75} S$$

The suppression factor, S is required to account for the fact that nucleation is more strongly suppressed when the macroscopic convective effect increases in strength. To calculate this suppression factor, Chen used a regression analysis of the data to fit S as a

function of a two phase Reynolds number defined as:

$$\mathrm{Re}_{tp} = \mathrm{Re}_l [F(X_{tt})]^{1.25}$$

Chen originally presented the suppression data in graphical format. However, Collier [ref] found the following empirical fit for the suppression factor (which is used in this study):

$$S(\mathrm{Re}_{tp}) = \left(1.25 + 2.56 x 10^{-6} \mathrm{Re}_{tp}^{1.17}\right)^{-1}$$

Collier, also, provided empirical fits for the F(Xtt) data in the form:

$F(X_{tt}) = 1$ for $X_{tt}^{-1} \le 0.1$

$F(Xtt) = 2.35 \left(0.213 + \frac{1}{X_{tt}}\right)^{0.736}$ for $X_{tt}^{-1} > 0.1$

The Martinelli parameter Xtt is calculated as:

$$X_{tt} = \left(\frac{1-x}{x}\right)^{0.9} \left(\frac{\rho_g}{\rho_l}\right)^{0.5} \left(\frac{\mu_l}{\mu_g}\right)^{0.1}$$

B) KANDLIKAR CORRELATION (2004)

Can be summarized as:

1. Turbulent Region: $\mathrm{Re}_{LO} \ge 3000$

$$h_{TP,NBD} = 0.6683 Co^{-0.2} (1-x)^{0.8} f_2(Fr_{LO}) h_{LO} + 1058 Bo^{0.7} (1-x)^{0.8} F_{Fl} h_{LO}$$
$$h_{TP,CBD} = 1.136 Co^{-0.9} (1-x)^{0.8} f_2(Fr_{LO}) h_{LO} + 667.2 Bo^{0.7} (1-x)^{0.8} F_{Fl} h_{LO}$$

Where:

$f_2(Fr_{LO}) = (25 Fr_{LO})^{0.3}$ *if horizontal and* $Fr_L \le 0.04$

$f_2(Fr_{LO}) = 1$ *if vertical or* $Fr_L > 0.04$

$$h_{LO} = \frac{\mathrm{Re}_{LO} \mathrm{Pr}_L (f/2)(K_L/D)}{1 + 12.7(\mathrm{Pr}_L^{2/3} - 1)(f/2)^{0.5}} \quad for \quad 10^4 \le \mathrm{Re} \le 5 \times 10^6$$

$$h_{LO} = \frac{(\mathrm{Re}_{LO} - 1000) \mathrm{Pr}_L (f/2)(K_L/D)}{1 + 12.7(\mathrm{Pr}_L^{2/3} - 1)(f/2)^{0.5}} \quad for \quad 3000 \le \mathrm{Re} \le 10^4$$

$$f = [1.58 \ln(\mathrm{Re}_{LO}) - 3.28]^{-2}$$

hTP = greater of $(h_{TP,NBD}, h_{TP,CBD})$

2. Transitional Flow Region: $1600 \le \mathrm{Re}_{LO} \le 3000$

$$h_{TP,NBD} = 0.6683\, Co^{-0.2} (1-x)^{0.8}\, h_{LO} + 1058\, Bo^{0.7} (1-x)^{0.8} F_{Fl}\, h_{LO}$$

$$h_{TP,CBD} = 1.136\, Co^{-0.9} (1-x)^{0.8}\, h_{LO} + 667.2\, Bo^{0.7} (1-x)^{0.8} F_{Fl}\, h_{LO}$$

With h_{LO} taken from linear interpolation between the turbulent value using Gnielinski equation and the laminar value using $h_{LO} = (Nu*K/D_h)$

h_{TP} = greater of $\left(h_{TP,NBD}, h_{TP,CBD}\right)$

3. Laminar Flow Region: $\mathrm{Re}_{LO} \le 1600$

$$h_{TP,NBD} = 0.6683\, Co^{-0.2} (1-x)^{0.8}\, h_{LO} + 1058\, Bo^{0.7} (1-x)^{0.8} F_{Fl}\, h_{LO}$$

$$h_{TP,CBD} = 1.136\, Co^{-0.9} (1-x)^{0.8}\, h_{LO} + 667.2\, Bo^{0.7} (1-x)^{0.8} F_{Fl}\, h_{LO}$$

$h_{LO} = (Nu*K/D_h)$

h_{TP} = greaterof $\left(h_{TP,NBD}, h_{TP,CBD}\right)$

4. Low Reynolds Number Flow in Minichannels:

$100 \le \mathrm{Re}_{LO} \le 410$

$$h_{TP,NBD} = 0.6683\, Co^{-0.2} (1-x)^{0.8}\, h_{LO} + 1058\, Bo^{0.7} (1-x)^{0.8} F_{Fl}\, h_{LO}$$

$$h_{TP,CBD} = 1.136\, Co^{-0.9} (1-x)^{0.8}\, h_{LO} + 667.2\, Bo^{0.7} (1-x)^{0.8} F_{Fl}\, h_{LO}$$

$h_{LO} = (Nu*K/D_h)$

h_{TP} = larger of $\left(h_{TP,NBD}, h_{TP,CBD}\right)$

5. Very Low Reynolds Number in Microchannels:

$\mathrm{Re}_{LO} \le 100$

$$h_{TP,NBD} = 0.6683\, Co^{-0.2} (1-x)^{0.8}\, h_{LO} + 1058\, Bo^{0.7} (1-x)^{0.8} F_{Fl}\, h_{LO}$$

Where: $h_{LO} = (Nu*K/D_h)$

In this region: $h_{TP} = h_{TP,NBD}$

C) GUNGOR-WINTERTON CORRELATION (1986)

The form of the correlation is as follows:

$$h = Eh_l + Sh_{nb}$$

l: liquid only

nb:Nucleate boiling

The factor E is termed the enhancement factor and is given via:

$$E = 1 + 24000\, Bo^{1.16} + 1.37\left(\frac{1}{\chi_{tt}}\right)^{0.86}$$

where χ_{tt} is the martinelli parameter

$$S = \left(1 + 0.00000115\, E^2\, \mathrm{Re}_l^{1.17}\right)^{-1}$$

And the nucleate boiling heat transfer coefficient is calculated using the Copper correlation:

$$h_{nb} = 55 p_r^{0.12} \left(-\log_{10} p_r\right)^{-0.55} M^{-0.5} q^{0.67}$$

D) GUNGOR-WINTERTON REVISED CORRELATION (1987)

This simpler form of the Gungor-Winterton correlation is given by:

$$h = h_l \left[1 + 3000\, Bo^{0.86} + \left(\frac{x}{1-x}\right)^{0.75} \left(\frac{\rho_l}{\rho_v}\right)^{0.41}\right]$$

E) SHAH CORRELATION (1977)

For Shah Correlation the heat transfer coefficient takes the form:

$$\psi_s = \frac{h}{h_l} = f\left(Co, Bo, Fr_{le}\right)$$

With the relevant dimensionless parameters provided as:

$$Co = \left(\frac{1-x}{x}\right)^{0.8} \left(\frac{\rho_v}{\rho_l}\right)^{0.5}$$

$$Bo = \frac{q''}{G h_{lv}}$$

$$Fr_{le} = \frac{G^2}{\rho_l^2 g D}$$

The original Shah correlation was presented in graphical form. In 1982 Shah provided a computational representation of his correlation. This computational representation was outlined in [ref]:

$N_s = Co$ for $\mathrm{Fr}_{le} \ge 0.04$

$N_s = 0.038\, Fr_{le}^{-0.3} Co$ for $\mathrm{Fr}_{le} < 0.04$

$F_s = 14.7$ for $\mathrm{Bo} \ge 11\mathrm{E}-4$

$F_s = 15.4$ for $\mathrm{Bo} < 11\mathrm{E}-4$

$$\psi_{cb} = 1.8 N_s^{-0.8}$$

For Ns > 1

$\psi_{nb} = 230\, Bo^{0.5}$ for $\mathrm{Bo} > 0.3\mathrm{E}-4$

$$\psi_{nb} = 1 + 46\, Bo^{0.5}$$

for $\mathrm{Bo} \le 0.3\mathrm{E}-4$

$$\psi_s = \max\left(\psi_{cb}, \psi_{nb}\right)$$

For Ns =< 1

$$\psi_{bs} = F_s \mathrm{Bo}^{0.5} \exp\left(2.74 \mathrm{N}_s^{-0.1}\right)$$

$$\text{for } 0.1 < \mathrm{N}_s \leq 1$$

$$\psi_{bs} = F_s \mathrm{Bo}^{0.5} \exp\left(2.47 \mathrm{N}_s^{-0.15}\right)$$

$$\text{for } \mathrm{N}_s \leq 0.1$$

The computational representation is used in this study.